energies

MDPI

Article

A Theoretical Analysis of Mobility Detection in Connectivity-Based Localization for Short-Range Networks

Sangwoo Lee [1,*], Ilmu Byun [2], Sungjin Kim [3] and Sunwoo Kim [3,*]

[1] KPS Technology Team, Korea Aerospace Research Institute, Daejeon 34133, Korea
[2] Korea Railroad Research Institute, Uiwang 16105, Korea; ilmubyun@krri.re.kr
[3] Department of Electronics and Computer Engineering, Hanyang University, Seoul 04763, Korea; stingsungs@hanyang.ac.kr
* Correspondence: lswoo@kari.re.kr (S.L.); remero@hanyang.ac.kr (S.K.)

Abstract: This paper presents a theoretical analysis of mobility detection in connectivity-based localization, which exploits connectivity information as range measurements to anchors at a known location, to investigate how well and how precise mobility can be detected with connectivity in short-range networks. We derive mobility detection, miss detection, and false alarm probabilities in terms of a mobility detection threshold, defined as the minimum distance to detect the mobility, under the shadow fading channel and arbitrary mobility models to take into account practical and general scenarios. Based on the derivations, we address the threshold determination with the criteria in the sense of the minimum average error from miss detection and false alarm. Numerical and simulation evaluations are performed to verify our theoretical derivations, to show that increasing anchor numbers can improve the mobility detection probability with a smaller detection threshold, and that the probabilities are bounded by the weights of miss detection and false alarm. This work is the first attempt at addressing the performance of mobility detection using connectivity, and it can be utilized as a baseline for connectivity-based mobility tracking.

Keywords: connectivity-based localization; mobility detection; mobility tracking; theoretical analysis

Citation: Lee, S.; Byun, I.; Kim, S.; Kim, S. A Theoretical Analysis of Mobility Detection in Connectivity-Based Localization for Short-Range Networks. *Energies* **2021**, *14*, 1162. https://doi.org/10.3390/en14041162

Academic Editor: Javier Contreras

Received: 7 December 2020
Accepted: 18 February 2021
Published: 22 February 2021

1. Introduction

Connectivity-based localization has been highlighted for wireless networks with short-range communications (e.g., WiFi, Bluetooth, and Zigbee) where explicit range measurements such as time-of-arrival, time-difference-of-arrival, and angle-of-arrival are not available due to systematic and/or cost reasons or where the range measurements are likely to be severely corrupted due to environmental reasons [1]. The importance of connectivity-based localization is also increasing with the fast-growing IoT (Internet-of-Things) applications based on device-to-device communication and mesh networking capabilities [2]. Since connectivity is an implicit (on/off) range measurement that tells if one is placed within the communication range of another, connectivity-based localization is known to provide a coarse-grained location. Nevertheless, it is still effective and fascinating for many applications such as environment monitoring, patient monitoring, and theft surveillance that are satisfied with space-level accuracy (depending on the communication range and scenarios, space may correspond to room, building, zone, block, or others), while having strict requirements for simple implementations (the demand on simplicity in implementation generally arises from the limitations on computation power and processing capabilities of devices as well as overall cost) and robustness against non-predictable channel variations. In addition, connectivity-based localization can be utilized to complement range-based localization for reducing the search region and convergence time (i.e., time-to-first-fix) [3,4], which are critical factors for real implementations.

Pioneering efforts focused on the localization problem in static wireless sensor networks, targeting environment monitoring applications where none of the nodes including

blueanchors, which are placed at perfectly known locations and act as references for node localization, are moving once deployed. Routers, also referred to as access points in a more general sense, typically play the role of anchor in WiFi networks, while special nodes acting as anchors are called as beacons in Bluetooth and Zigbee. The terms are interchangeably used with seed nodes in the field of wireless sensor networks. The most straightforward approach [5] to the static localization problem is to provide the centroid of directly heard (seen) anchors, which are referred to as one-hop anchors. However, it is well-known that the centroid has low accuracy and low availability. It is worth noting that there is a trade-off between accuracy and availability since accuracy is inversely proportional to and availability is proportional to the transmission ranges of the anchors. To overcome the drawbacks of the centroid, Niculescu and Nath proposed the Distance Vector-Hop (DV-Hop) algorithm [6] applying a multihop fashion and multilateration where the distance to each anchor is computed as the product of the hop counts to the anchor and the average distance per hop, which is the ratio of the sums of distances and hop counts between the anchors. This is feasible in isotropic networks where the shortest path of any node pair forms a linear shape, but fragile in practice due to the network anisotropy (e.g., non-uniform node deployments, irregular radio propagation) [2,7]. Many modifications of the DV-Hop algorithm have been made to deal with the anisotropy issues by deriving new average distances per hop [8–14], by refining the distance [7,9,15,16] and location estimates [14,17–19], and/or by selecting reliable anchors [10,20–22] with understanding of the path and topology properties. Further details are available in [7,23,24].

As a variety of mobile applications have been introduced, mobility (location) tracking has become more challenging. To resolve the connectivity-based mobility (location) tracking problem, Hu and Evans [25] proposed a Monte Carlo localization (MCL) algorithm using random particles. More specifically, the MCL algorithm randomly deploys particles within a circle centered at the previous location estimate with a radius of the maximum distance movable in a discrete unit time and computes the centroid of those valid particles that are placed within the coverage of two-hop anchors under the unit disk graph (UDG) model [26], which is an ideal channel model not taking into account any uncertainties during propagation. In [27], the concept of building a bounding box was adopted to reduce the computational complexity from the particles that are filtered out by the anchors and not used for tracking, and further modifications were made to narrow down the bounding box for achieving higher computational efficiency by imposing more constraints from the information of one/two-hop anchors [28–31], neighboring nodes [28,30], historical anchors [32,33], and/or historical location estimates [31]. It is obvious that as the dimension of the constraints increases, a smaller box is drawn and results in improvement in not only computational efficiency, but also tracking accuracy. However, they all have missed one important point: that the underlying assumption on the maximum movable distance can adversely affect the performance, and the worst case occurs when a node is not moving. To handle this issue, it is necessary to determine whether a node has moved or not, which is referred to as the mobility detection problem in this paper.

Theoretical studies, of which results serve as baselines for designing localization systems in mobile scenarios, have been also made to measure lower bounds on localization errors caused by movements that cannot be detected with connectivity information [34–37]. The concept of the lower error bound was first defined in [34] as the expectation of a maximum movable distance that does not bring changes in connectivity to the anchors. Here, the maximum movable distance was defined with the areas that other anchors do not exist under a Poisson node distribution and the UDG radio model [26]. MacLean and Datta [35] pointed out that the result of [34] is only applicable for scenarios with small movements, and they presented a new lower bound that incorporates errors from a large movement. The lower bound due to a small movement was revisited under a shadow fading channel model in [36] to consider practical aspects. Gui et al. [37] proposed algorithmic methods to compute lower bounds for real deployments in both UDG and fading models, while the ones derived in [34–36] are fully probabilistic bounds. As none of

the previous works has addressed the mobility detection problem in connectivity-based localization, no theoretical studies on mobility detection have been done, while the former theoretical studies [34–37] have focused on the accuracy perspective.

This paper is the first to address the connectivity-based mobility detection problem and to build theoretical foundations which will open up new possibilities in both the academic and industrial fields of research and application. We first provide a general framework of the connectivity-based mobility detection in terms of a mobility detection threshold. Based on this framework, three performance metrics, which are mobility detection, miss detection, and false alarm probabilities, are defined and derived under the shadow fading channel model and arbitrary mobility models. We then discuss the threshold determination from the perspective of minimizing the average error with respect to miss detection and false alarm. The results from this work can serve as a technical guide for designing connectivity-based localization systems in mobile scenarios; for example, deriving the minimum number of anchors to achieve a specific resolution (detection threshold) required for an application.

The remainder of this paper is organized as follows. Section 2 describes the system and channel models. Section 3 provides the definition and derivation of mobility detection, miss detection, and false alarm probabilities. Section 4 addresses the determination of the mobility detection threshold. Section 5 provides numerical results to validate the theoretical foundations. Section 6 concludes this paper along with discussions on future work.

Notation: Throughout the paper, vectors and matrices are denoted by lowercase and uppercase bold letters, respectively. The superscript T denotes the transpose operation. The cardinal number of a set is denoted by $|\cdot|$. The Euclidean norm of a vector is denoted by $||\cdot||$. $\mathbb{E}[\cdot]$ represents the expectation of a random vector. $\mathcal{N}(\mathbf{u}, \mathbf{\Sigma})$ represents a normal distribution with mean $\mathbf{u}$ and covariance $\mathbf{\Sigma}$. $\phi(\cdot)$ denotes the probability density function (PDF) of the standard normal distribution and $\Phi(\cdot)$ is its cumulative distribution function (CDF).

2. System and Channel Models

We consider a mobile node to be localized with the aid of multiple anchors at known locations in a two-dimensional circular space, denoted by $\mathcal{S}$, with a radius of R [36]. The anchors are randomly deployed according to a Poisson distribution with rate λ. Under the Poisson deployment, the number of anchors is represented by a random variable A with $\mu_A \triangleq \mathbb{E}[A] = \lambda\pi R^2$. The anchors are assumed to be stationary once they are deployed at known points, denoted by $\{\mathbf{p}_1, \mathbf{p}_2, \ldots, \mathbf{p}_A\}$ where $\mathbf{p}_a = [x_a, y_a]^T$ is the location of the a-th anchor. It is worth noting that a single mobile node is assumed for the sake of simplicity, but the scenario can be simply extended to multiple mobile nodes without any additional assumption.

At any time n, the location of the mobile node is denoted by $\mathbf{m}_n = [x_n, y_n]^T$, and the distance from the mobile node to the a-th anchor is defined as $d_{a,n} = ||\mathbf{p}_a - \mathbf{m}_n||$. Then, the received signal power (in dBm) is expressed as [38]

$$r_{a,n} = r_{a,0} - 10\eta \log_{10} \frac{d_{a,n}}{d_{a,0}} + v_{a,n}, \tag{1}$$

where $r_{a,0}$ is the received signal power (in dBm) at the reference distance $d_{a,0}$ (typically, 1m for short-range communications [39,40]) for the a-th anchor, η is the path loss exponent, and $v_{a,n} \sim \mathcal{N}(0, \sigma^2)$ is a zero-mean Gaussian random variable with variance σ^2 representing the shadowing effect. The connectivity between the mobile node and the a-th anchor is assumed to be made if $r_{a,n} \geq \gamma$ where γ is a signal level threshold, typically corresponding to the required signal-to-noise-ratio for data decoding. This model is typically adopted for both line-of-sight and non-line-of-sight propagation in short-range communications and can be found in related literature [39,40] as well as in the ITU (International Telecommunication Union) recommendations (e.g., ITU-R P.1238 [41] and P.1411 [42]). The parameters in (1) have different values with respect to wireless communications systems and device specifications, and it is also known that the values are different across oper-

ational areas and over time due to environmental changes (e.g., temperature, humidity, properties of obstacles) [2,38]. According to the recent works [39,40], it has been reported that $r_{a,0} \in [-68.99, -56]$, $\eta \in [1.87, 2.87]$, $\sigma \in [0.20, 4.60]$ for Bluetooth Low Energy (BLE). Typical values of γ are in the ranges of $[-95, -70]$ for BLE [43] and of $[-100, -85]$ for IEEE 802.15.4 [44].

It is assumed that the shadow fading effects at subsequent times n and $n+1$ are correlated and modeled as a bivariate normal distribution as follows:

$$f_{\mathbf{v}_{a,n}}(\mathbf{v}_{a,n}) = \frac{1}{2\pi\sigma^2\sqrt{1-\rho(z_n)^2}} \exp\left(-\frac{||\mathbf{v}_{a,n}||^2 - 2\rho(z_n)v_{a,n}v_{a,n+1}}{2\sigma^2(1-\rho(z_n)^2)}\right), \tag{2}$$

where $\mathbf{v}_{a,n} = [v_{a,n}, v_{a,n+1}]^T$, $z_n = \|\mathbf{m}_n - \mathbf{m}_{n+1}\|$, and $\rho(z_n)$ is the spatio-tempral correlation between $v_{a,n}$ and $v_{a,n+1}$. According to [38], $\rho(z_n)$ is given as

$$\rho(z_n) = \exp\left(-\frac{z_n}{d_{\text{dec}}} - \tau\right), \tag{3}$$

where d_{dec} is the decorrelation distance and τ is a temporal correlation coefficient, normalized by a sampling period.

3. Theoretical Foundations of Mobility Detection in Connectivity-Based Localization

3.1. Definition of Mobility Detection, Miss Detection, and False Alarm Probabilities

The fundamental idea behind connectivity-based localization is to provide the feasible region where the mobile node can be located by translating γ into the maximum achievable distance $d_{\max}$ to communicate with an anchor based on (1). The location is then typically estimated to be the centroid of the feasible region drawn by multiple anchors in the least squares sense [45]. This yields that mobility can be detected from a change in the feasible region. In other words, the mobile node is considered having moved if the node finds at least one anchor whose connectivity has changed in a subsequent time interval. Making a decision with only information in a subsequent time interval (he dimension of measurements is two) may be inappropriate in practice where the changes in connectivity can occur due to sudden appearance/disappearance of moving obstacles and radio interference, even though the mobile node has not moved. A practical strategy to handle this issue is to increase the number of measurements by extending the observation period and to test if the number of changes exceeds a threshold. This strategy is simple and effective to mitigate the effect of such unexpected cases so that it is typically adopted in many studies and designs [7,46,47]. However, in this paper, we consider a system using two subsequent measurements for mobility detection to build a theoretical framework providing foundations for further research.

To provide intuitive insights on the connectivity-based mobility detection, a simple example is presented in Figure 1 where the mobile node is tracked with three anchors of which the maximum achievable distances are denoted by the dashed line under the absence of uncertainties in signal levels. As long as the mobile node moves within the colored area where the node maintains the connectivity with all the anchors, its mobility cannot be detected; otherwise, the mobility can be simply detected by any connectivity-based localization algorithms. The minimum distance to detect the mobility for a certain level of performance is typically defined as the resolution, denoted by ϵ, which is determined depending on propagation characteristics and system configurations including anchor numbers, anchor deployments, and others. It is also worth noting that ϵ can be understood as the threshold to decide if the node is moving for a subsequent time period from the detection interpretation.

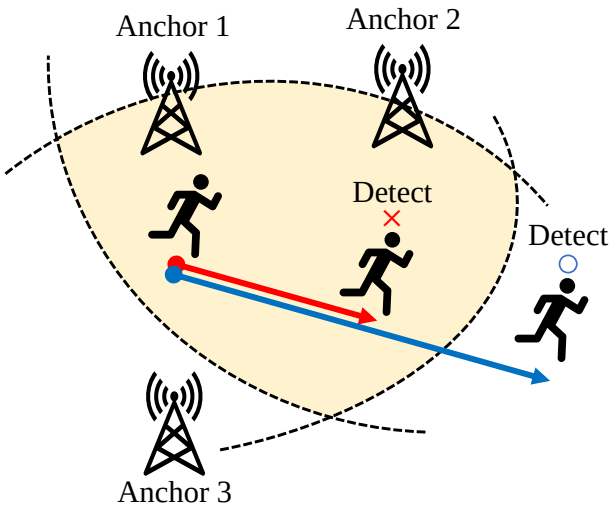

Figure 1. A conceptual illustration of mobility detection in connectivity-based localization.

By defining ϵ, we can construct the following simple hypothesis in terms of the movement, denoted by z_n, during the time interval of n and $n+1$:

$$\begin{aligned} \mathcal{H}_0 &: z_n \in [0, \epsilon], \\ \mathcal{H}_1 &: z_n \in (\epsilon, R]. \end{aligned} \tag{4}$$

From the connectivity establishment condition $r_{a,n} \geq \gamma$, we have two cases that change connectivity in the subsequent time interval: i) $r_{a,n} \geq \gamma$ and $r_{a,n+1} < \gamma$; and ii) $r_{a,n} < \gamma$ and $r_{a,n+1} \geq \gamma$. Let $\mathcal{T}$ be the set of anchors whose connectivity with the mobile node changes, and it can be defined as

$$\mathcal{T} \triangleq \{a \mid (r_{a,n} - \gamma)(r_{a,n+1} - \gamma) < 0, \ \forall a\}. \tag{5}$$

When the mobile node moves by z_n, the probability that connectivity between the mobile node and the a-th anchor does not change is simply derived from (2), which is given by

$$\begin{aligned} \Pr(a \in \mathcal{T} \mid Z = z_n) &\triangleq \Pr(r_{a,n} \geq \gamma, r_{a,n+1} \geq \gamma) + \Pr(r_{a,n} < \gamma, r_{a,n+1} < \gamma) \\ &= 1 - Q\left(\frac{\bar{r}_{a,n} - \gamma}{\sigma}\right) - Q\left(\frac{\bar{r}_{a,n+1} - \gamma}{\sigma}\right) + 2F_{\mathbf{V}_{a,n}}(\boldsymbol{\gamma}_{a,n}). \end{aligned} \tag{6}$$

where $Q(\cdot)$ is the Q-function, $F_{\mathbf{V}_{a,n}}(\mathbf{v}_{a,n})$ is the CDF of $\mathbf{V}_{a,n}$, $\boldsymbol{\gamma}_{a,n} = [\gamma - \bar{r}_{a,n}, \gamma - \bar{r}_{a,n+1}]^T$, and $\bar{r}_{a,n} = \mathbb{E}[r_{a,n}]$.

Recall that in the connectivity-based localization, the node is considered in moving when the connectivity with at least one anchor changes. Mathematically, it can be expressed as $|\mathcal{T}| > 0$. Accordingly, the probabilities of mobility detection $P_D(\epsilon)$, miss detection $P_M(\epsilon)$, and false alarm $P_F(\epsilon)$ are respectively defined as

$$\begin{aligned} P_D(\epsilon) &\triangleq \Pr(|\mathcal{T}| > 0 \mid \mathcal{H}_1) = 1 - P_M(\epsilon), \\ P_M(\epsilon) &\triangleq \Pr(|\mathcal{T}| = 0 \mid \mathcal{H}_1), \\ P_F(\epsilon) &\triangleq \Pr(|\mathcal{T}| > 0 \mid \mathcal{H}_0) = 1 - \underbrace{\Pr(|\mathcal{T}| = 0 \mid \mathcal{H}_0)}_{\text{correct rejection}}. \end{aligned} \tag{7}$$

3.2. Derivation of P_D, P_M, and P_F

Given the PDF $f_Z(z)$ and CDF $F_Z(z)$ for the movement $0 \leq Z \leq R$, $\Pr(\mathcal{H}_0) = \Pr(0 \leq Z \leq \epsilon) = F_Z(\epsilon)$ and $\Pr(\mathcal{H}_1) = \Pr(\epsilon < Z \leq R) = 1 - F_Z(\epsilon)$. Then, the three probabilities are simply derived as

$$P_D(\epsilon) = 1 - \frac{\Pr(|\mathcal{T}| = 0, \epsilon < Z \leq R)}{1 - F_Z(\epsilon)}, \tag{8}$$

$$P_M(\epsilon) = \frac{\Pr(|\mathcal{T}| = 0, \epsilon < Z \leq R)}{1 - F_Z(\epsilon)}, \tag{9}$$

$$P_F(\epsilon) = 1 - \frac{\Pr(|\mathcal{T}| = 0, 0 \leq Z \leq \epsilon)}{F_Z(\epsilon)}, \tag{10}$$

where (8) and (9) hold for $F_Z(\epsilon) < 1$, and (10) is feasible for $F_Z(\epsilon) > 0$. Here,

$$\begin{aligned} \Pr(|\mathcal{T}| = 0, \epsilon < Z \leq R) &= \int_{\epsilon}^{R} \Pr(|\mathcal{T}| = 0, Z = z_n)\, dz_n \\ &= \int_{\epsilon}^{R} f_Z(z_n) \Pr(|\mathcal{T}| = 0 | Z = z_n)\, dz_n, \end{aligned} \tag{11}$$

$$\begin{aligned} \Pr(|\mathcal{T}| = 0, 0 \leq Z \leq \epsilon) &= \int_{0}^{\epsilon} \Pr(|\mathcal{T}| = 0, Z = z_n)\, dz_n \\ &= \int_{0}^{\epsilon} f_Z(z_n) \Pr(|\mathcal{T}| = 0 | Z = z_n)\, dz_n. \end{aligned} \tag{12}$$

Under the Poisson anchor deployment, $\Pr(|\mathcal{T}| = 0 | Z = z_n)$ and $h(z_n)$ are given as [36]

$$\Pr(|\mathcal{T}| = 0 \mid Z = z_n) = \exp\{\mu_A (h(z_n) - 1)\}, \tag{13}$$

$$h(z_n) = \oint_{\mathcal{S}} \frac{d_{a,n}}{\pi R^2} \Pr(a \in \mathcal{T} \mid Z = z_n)\, d\mathcal{S}. \tag{14}$$

$h(z_n)$ cannot be expressed in a closed form, but it can be calculated with computer simulations using a Monte Carlo method and simple curve fitting methods. Figure 2 shows the changes of $h(z_n)$ with respect to z_n and σ, computed with Monte Carlo simulations, where $R = 100$, $d_{a,0} = 1$, $d_{\text{cor}} = 2$, $\tau = 1$, and $\eta = 2.2$. It is obviously seen that $h(z_n)$ decreases with larger z_n and higher σ, which lead to a larger difference in received signal power in the subsequent time interval. After the computation of $h(z_n)$, $P_D(\epsilon)$, $P_M(\epsilon)$, and $P_F(\epsilon)$ derived in (8)–(10) can be further computed.

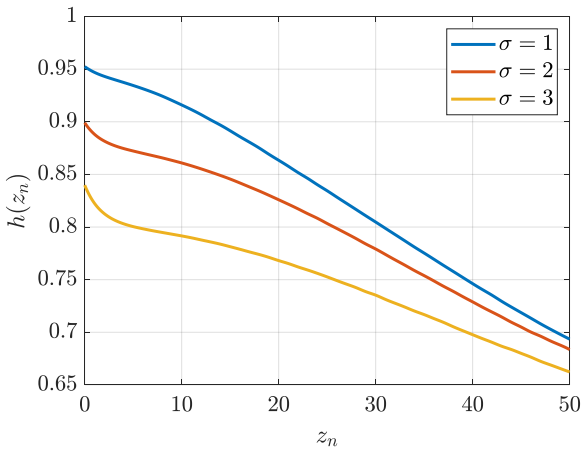

Figure 2. The changes of $h(z_n)$ with respect to z_n and σ.

For $F_Z(\epsilon) = 1$, $P_D(\epsilon)$ and $P_M(\epsilon)$ are defined as

$$P_D(\epsilon) = 1 - \underbrace{\exp\{\mu_A(h(\epsilon) - 1)\}}_{P_M(\epsilon)} \tag{15}$$

using the L'Hospital's rule (see Appendix A for the proof) and $P_F(\epsilon)$ becomes

$$P_F(\epsilon) = 1 - \mathbb{E}[\exp\{\mu_A(h(z_n) - 1)\}] \tag{16}$$

since $f_Z(z) > 0$ only for $0 \leq z \leq \epsilon$. Similarly, for $F_Z(\epsilon) = 0$,

$$P_D(\epsilon) = 1 - \underbrace{\mathbb{E}[\exp\{\mu_A(h(z_n) - 1)\}]}_{P_M(\epsilon)} \tag{17}$$

and

$$P_F(\epsilon) = 1 - \exp\{\mu_A(h(\epsilon) - 1)\}. \tag{18}$$

The proof of (18) appears in Appendix B.

3.3. Asymptotic Analysis

When $\sigma \to \infty$, (2) is approximated to a uniform distribution over all feasible values of $\mathbf{v}_{a,n}$ and both (6) and (14) converge to $1/2$. In other words, the probabilities of connectivity to any anchor being maintained and being changed are exactly half and half regardless of the movement, even if the separation to the anchor is very small. This yields

$$\Pr(|\mathcal{T}| = 0, \epsilon < Z \leq R) = \int_{\epsilon}^{R} f_Z(z_n) \exp\left(-\frac{\mu_A}{2}\right) dz_n = \{1 - F_Z(\epsilon)\} \exp\left(-\frac{\mu_A}{2}\right), \tag{19}$$

$$\Pr(|\mathcal{T}| = 0, 0 \leq Z \leq \epsilon) = \int_{0}^{\epsilon} f_Z(z_n) \exp\left(-\frac{\mu_A}{2}\right) dz_n = F_Z(\epsilon) \exp\left(-\frac{\mu_A}{2}\right). \tag{20}$$

By substituting (19) and (20) into (8)–(10), the asymptotic performance of $P_D(\epsilon)$, $P_M(\epsilon)$, and $P_F(\epsilon)$ is given as

$$P_D^{\infty}(\epsilon) = P_F^{\infty}(\epsilon) = 1 - \exp\left(-\frac{\mu_A}{2}\right) \quad \text{and} \quad P_M^{\infty}(\epsilon) = \exp\left(-\frac{\mu_A}{2}\right). \tag{21}$$

It is a general principle that the probability of connectivity being changed increases as the channel variation becomes more severe due to multipath and other interference. In addition, the more anchors there are, the lower probability that $|\mathcal{T}| = 0$. As a consequence, the probability that the mobile node says in moving gradually increases with the number μ_A of anchors even though $z_n \leq \epsilon$ and $F_Z(\epsilon) \approx 1$. This implies the reduction in the probability of determining $\mathcal{H}_0$. Thus, it can be clearly seen in (21) that the detection and false alarm probabilities increase while the miss detection probability decreases with increasing the anchor numbers.

4. Threshold Determination for Minimizing the Average Error

A threshold in a detection problem is typically determined as the likelihood ratio, while the detection threshold ϵ in our problem is a design parameter to be set properly depending on system settings and applications. In this section, we discuss how to set the best ϵ, denoted by ϵ_0, from the perspective of minimum average error cost under zero cost for making right decisions.

Given a priori probabilities $\Pr(\mathcal{H}_0)$ and $\Pr(\mathcal{H}_1)$, the average error cost $C_e(\epsilon)$ arising from the wrong decisions (i.e., miss detection and false alarm) is

$$C_e(\epsilon) \triangleq \alpha \Pr(\mathcal{H}_1) P_M(\epsilon) + (1 - \alpha) \Pr(\mathcal{H}_0) P_F(\epsilon), \tag{22}$$

where $0 \leq \alpha \leq 1$ is the cost for miss detection, and $1-\alpha$ corresponds to the cost for false alarm. In addition to ϵ, the cost α is another factor that controls the overall cost and further detection probabilities. We show that the probabilities are bounded by α at the end of this section. The selection of α is also discussed with numerical analysis in Section 5. Substituting (8)–(10) into (22) yields

$$\begin{aligned} C_e(\epsilon) = \alpha \int_{\epsilon}^{R} f_Z(z_n) \exp\{\mu_A(h(z_n)-1)\}\, dz_n \\ + (1-\alpha)\left[F_Z(\epsilon) - \int_0^{\epsilon} f_Z(z_n)\exp\{\mu_A(h(z_n)-1)\} dz_n\right]. \end{aligned} \tag{23}$$

As the cost changes in terms of ϵ, which determines the integration region, the problem is then formulated to find ϵ_0 minimizing (23), which is either increasing or decreasing or convex with respect to ϵ. The behavior of (23) can be determined by using the first derivative test:

$$\frac{\partial C_e(\epsilon)}{\partial \epsilon} = f_Z(\epsilon)[(1-\alpha) - \exp\{\mu_A(h(\epsilon)-1)\}] \gtrless 0. \tag{24}$$

(23) is increasing if (24) has always a positive value for any ϵ, which is given as

$$(1-\alpha) - \exp\{\mu_A(h(\epsilon)-1)\} > 0. \tag{25}$$

Since $h(\epsilon) \leq 1$ is a probability and is a decreasing function, as shown in Figure 2, (25) should hold for $\epsilon = 0$ at which $h(\epsilon)$ has the maximum value to (23) to be an increasing function, and this gives the condition for (23) being increasing:

$$\mu_A > \frac{\ln(1-\alpha)}{h(0)-1}. \tag{26}$$

Similarly, from $\partial \mathcal{C}_e(\epsilon)/\partial \epsilon < 0$, we can say that (23) is decreasing when

$$\mu_A < \frac{\ln(1-\alpha)}{h(R)-1}. \tag{27}$$

In addition, the average cost function is said to be convex and has the minimum value at

$$\epsilon_0 = h^{-1}\left(1 + \frac{\ln(1-\alpha)}{\mu_A}\right) \tag{28}$$

when

$$\frac{\ln(1-\alpha)}{h(R)-1} \leq \mu_A \leq \frac{\ln(1-\alpha)}{h(0)-1}. \tag{29}$$

Because $h(\epsilon)$ is decreasing, the convexity of (23) is guaranteed since the first derivative has a negative value in $\epsilon \in (0, \epsilon_0)$ and a positive value in $\epsilon \in (\epsilon_0, R)$ if the derivative becomes zero at ϵ_0. Therefore, we have

$$\epsilon_0 = \begin{cases} R, & \text{for } \mu_A < \dfrac{\ln(1-\alpha)}{h(R)-1}, \\ h^{-1}\left(1 + \dfrac{\ln(1-\alpha)}{\mu_A}\right), & \text{for } \dfrac{\ln(1-\alpha)}{h(R)-1} \leq \mu_A \leq \dfrac{\ln(1-\alpha)}{h(0)-1}, \\ 0, & \text{for } \mu_A > \dfrac{\ln(1-\alpha)}{h(0)-1}. \end{cases} \tag{30}$$

Figure 3 presents simulation results that show how ϵ_0 changes with respect to μ_A and α under the uniform random walk with a uniform direction (refer to (34)) and the settings

as the same as in Figure 2. It is clearly shown that ϵ_0 decreases exponentially with μ_A as expected from Figure 2 and (30). This indicates that increasing the number of anchors improves the detection resolution. In other words, the more anchors we use, the smaller movement we can detect. Another interesting observation is that α controls the change rate of ϵ_0. As α is set to a larger value, ϵ_0 decreases slowly with the increase of μ_A. This is because $\Pr(\mathcal{H}_1)P_M(\epsilon_0)$ remains dominant against $\Pr(\mathcal{H}_0)P_F(\epsilon_0)$ in (22) for a large value of α. For any $f_Z(z)$, $\Pr(\mathcal{H}_1)P_M(\epsilon_0)$ returns (11), which integrates a probability over $(\epsilon_0, R]$. Thus, ϵ_0 is required to be larger to minimize $\Pr(\mathcal{H}_1)P_M(\epsilon_0)$.

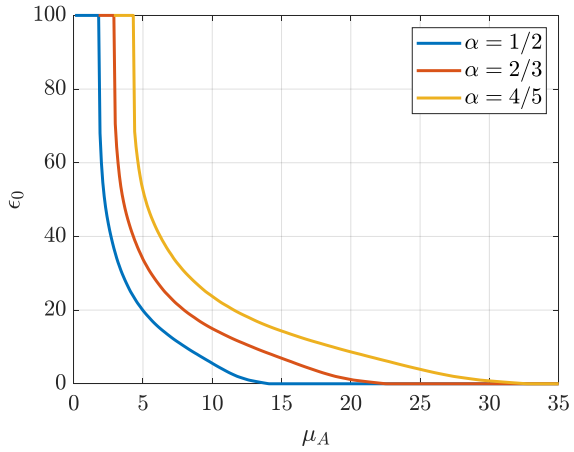

Figure 3. ϵ_0 under different μ_A and α.

Furthermore, the following propositions can be made with the results in Section 3 and show that the probabilities with (30) are bounded by α for $\frac{\ln(1-\alpha)}{h(R)-1} \leq \mu_A \leq \frac{\ln(1-\alpha)}{h(0)-1}$.

Proposition 1. *As $F_Z(\epsilon_0)$ approaches zero ($\epsilon_0 \to 0$ is a sufficient condition for $F_Z(\epsilon_0) \to 0$), $P_F(\epsilon_0)$ converges to α.*

Proof of Proposition 1. By substituting (28) into $P_F(\epsilon_0)$ in (18),

$$\lim_{F_Z(\epsilon_0)\to 0} P_F(\epsilon_0) = 1 - \exp\left\{\mu_A\left(1 + \frac{\ln(1-\alpha)}{\mu_A} - 1\right)\right\} = \alpha. \tag{31}$$

□

Proposition 2. *As $F_Z(\epsilon_0)$ approaches one ($\epsilon_0 \to R$ is a sufficient condition for $F_Z(\epsilon_0) \to 1$), $P_D(\epsilon_0)$ and $P_M(\epsilon_0)$ converge to α and $1-\alpha$, respectively.*

Proof of Proposition 2. By substituting (28) into P_D and P_M in (15),

$$\lim_{F_Z(\epsilon_0)\to 1} P_D(\epsilon_0) = 1 - \exp\left\{\mu_A\left(1 + \frac{\ln(1-\alpha)}{\mu_A} - 1\right)\right\} = \alpha, \tag{32}$$

$$\lim_{F_Z(\epsilon_0)\to 1} P_M(\epsilon_0) = \lim_{F_Z(\epsilon_0)\to 1} (1 - P_D(\epsilon_0)) = 1 - \alpha. \tag{33}$$

□

5. Numerical Results and Discussion

This section verifies and analyzes the theoretical results derived in Sections 3 and 4 through simulations and numerical evaluations using MATLAB. The settings for simulations and numerical evaluations are listed in Table 1. All the anchors are assumed to

be homogeneous, and the propagation characteristics are assumed to be the same such that $d_{1,0} = d_{2,0} = \cdots = d_{A,0}$ and $r_{1,0} = r_{2,0} = \cdots = r_{A,0}$. We adopt random walk mobility models for $f_Z(z)$, which are generally used to emulate tracking scenarios with a broad range of targets in nature move [48]. For simulations, a mobile node is placed at the origin, and anchors are randomly deployed with a Poisson distribution with varying μ_A in $\mathcal{S}$ centered at the origin with an area of πR^2. In each simulation, the mobile node moves along a random direction from the uniform probability over $[0, 2\pi]$ by a step length (travel distance) randomly drawn from random walk mobility models. In this paper, we assume a uniform random walk model whose PDF is given as

$$f_Z^U(z) = \begin{cases} \dfrac{1}{d_{\max}}, & \text{for } 0 \le z \le d_{\max}, \\ 0, & \text{for } d_{\max} < z \le R, \end{cases} \tag{34}$$

and a truncated Gaussian random walk model whose PDF is given as

$$f_Z^G(z) = \frac{\phi\left(\frac{z-\mu_Z}{\sigma_Z}\right)}{\sigma_Z\left\{\Phi\left(\frac{R-\mu_Z}{\sigma_Z}\right) - \Phi\left(-\frac{\mu_Z}{\sigma_Z}\right)\right\}} \quad \text{for } 0 \le z \le R \tag{35}$$

where μ_Z and σ_Z denote the mean of the travel distance and its standard deviation, respectively. Since anchors are assumed to be deployed with a Poisson distribution in this paper, the detection performance in all directions is almost the same in the case of node's movement made in a random direction with the uniform probability over $[0, 2\pi]$, and thus the effect of movement direction becomes negligible in our work.

Table 1. Parameters used in simulations and numerical evaluations.

Parameters	Descriptions	Values	References
R	Radius of space $\mathcal{S}$	100 m	-
η	Path loss exponent	2.2	[39,40]
σ	Noise level	1 dB	[39,40]
$d_{a,0}$	Reference distance for the a-th anchor	1 m	[40]
$r_{a,0}$	Received signal power for the a-th anchor at $d_{a,0}$	−68.99 dBm	[40]
d_{dec}	Decorrelation distance	2 m	[49]
τ	Temporal correlation coefficient, normalized by the sampling period	1	[49]
γ	Signal level threshold	−100 dBm	[44]
$d_{\max}$	Maximum communication range	∼50 m	Calculated by (1)

Figure 4 presents comparisons in $P_D(\epsilon_0)$, $P_M(\epsilon_0)$, and $P_F(\epsilon_0)$ between theoretical and simulation results to verify the theoretical calculations derived in Section 3. A total of 100,000 simulations were conducted for $\alpha = 0.5$ under the uniform random walk model. According to (29), μ_A was set to be between 3 and 14 to meet the convexity of (23), and the other parameters were set to the values in Table 1. We have clearly seen in Figure 4 that the theoretical calculations and simulations provide almost the same results. It is also seen that the increase in μ_A leads to both $P_D(\epsilon_0)$ and $P_F(\epsilon_0)$ increasing, but $P_M(\epsilon_0)$ decreases.

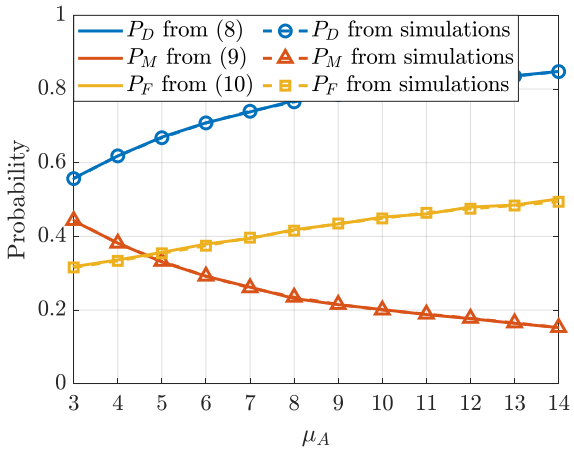

Figure 4. Comparisons in $P_D(\epsilon_0)$, $P_M(\epsilon_0)$, and $P_F(\epsilon_0)$ between theoretical and simulation results.

Assuming a Poisson distribution, a larger number of anchors indicates increasing the dimension of the constraints on the area where a node can be located. Here, the area is the region, denoted by the colored area in Figure 1, that connectivity to any anchor is not changing. Thus, as the dimension of the constraints is getting higher, we have a smaller area and higher detection resolution, that is, ϵ_0 becomes smaller as seen in Figure 3. The smaller area also implies that the node is nearly $d_{\max}$ away from some anchors, and the connectivity with those anchors is likely to change with signal fluctuations. In this sense, for $\Pr(\mathcal{H}_0) \leq \Pr(\mathcal{H}_1)$, $P_D(\epsilon_0)$ and $P_F(\epsilon_0)$ increase with the increase of μ_A, but $P_F(\epsilon_0)$ is upper-bounded by α as proved in the Proposition 1. For $\Pr(\mathcal{H}_0) > \Pr(\mathcal{H}_1)$, $P_M(\epsilon_0)$ increases while $P_D(\epsilon_0)$ and $P_F(\epsilon_0)$ decrease. Nevertheless, since $P_D(\epsilon_0)$ is lower-bounded by α and $P_M(\epsilon_0)$ is upper-bounded by $1-\alpha$ as proved in the Proposition 2, we can still control the detection performance by varying α.

The relevant results are presented in Figure 5 that shows the three probabilities under truncated Gaussian random walk models with $\mu_Z \in [0, 50]$. In this analysis, it is assumed that $\alpha = 0.5$, $\mu_A = 4$, and $\sigma_Z = 5$. ϵ_0 is then given to be 25.8 (near the median of the range of μ_Z) according to (28). As μ_Z becomes smaller compared to ϵ_0, $\Pr(\mathcal{H}_0) = F_Z(\epsilon_0)$ approaches one, and $P_D(\epsilon_0)$ has the minimum, but not goes to below α, referred to as the Proposition 2. Not only $P_D(\epsilon_0)$, but also $P_F(\epsilon_0)$, which is upper-bounded by α (referred to as the Proposition 1), has the maximum values for $\mu_Z = 50$ at which $\Pr(\mathcal{H}_0) = F_Z(\epsilon_0)$ becomes near zero. From the results, we can establish directions for selection of α depending on $z_{\min}$ that is a smallest value of z satisfying $F_Z(z_{\min}) = 1$ compared to ϵ_0. When $z_{\min} \ll \epsilon_0$, α should have a value larger than 0.5 to ensure $P_D(\epsilon_0) > P_M(\epsilon_0)$; otherwise, a lower value of α is preferable to minimize the upper bound of $P_F(\epsilon_0)$. Maximizing the overall performance such as the ratio $\Pr(\mathcal{H}_1)P_D(\epsilon_0)$ to $\Pr(\mathcal{H}_1)P_M(\epsilon_0)$ plus $\Pr(\mathcal{H}_0)P_F(\epsilon_0)$ may be a good option for selecting α. It is worth noting that approaches to the selection of α should be determined according to the system policy.

Figure 6 shows the cost function and the detection probability under the uniform random walk model with varying μ_A and α. All the other settings are the same as in Table 1. As discussed above, the decrease in ϵ_0 results in the increase in the gap between $\Pr(\mathcal{H}_0)$, which goes to zero, and $\Pr(\mathcal{H}_1)$, which goes to one, for a larger number of anchors under the uniform random walk model. Consequently, the concern of the miss detection remains dominant while the false alarm becomes insignificant in our mobility detection problem, which is reformulated as the problem of minimizing the miss detection. α also raises the weight on the miss detection. Thus, the cost function decreases and the detection probability increases over μ_A, and both increase with the increase in α. The corresponding $\Pr(\mathcal{H}_1)P_D(\epsilon_0)$, $\Pr(\mathcal{H}_1)P_M(\epsilon_0)$, and $\Pr(\mathcal{H}_0)P_F(\epsilon_0)$ are presented in Figure 7, which clearly shows that the overall detection performance is improved by increasing μ_A and setting a smaller value for α.

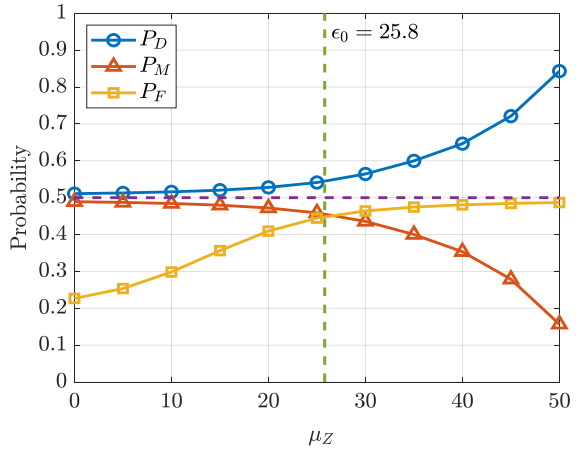

Figure 5. $P_D(\epsilon_0)$, $P_M(\epsilon_0)$, and $P_F(\epsilon_0)$ for $\mu_A = 4$ and $\alpha = 0.5$ under truncated Gaussian random walk models with different means of the travel distance.

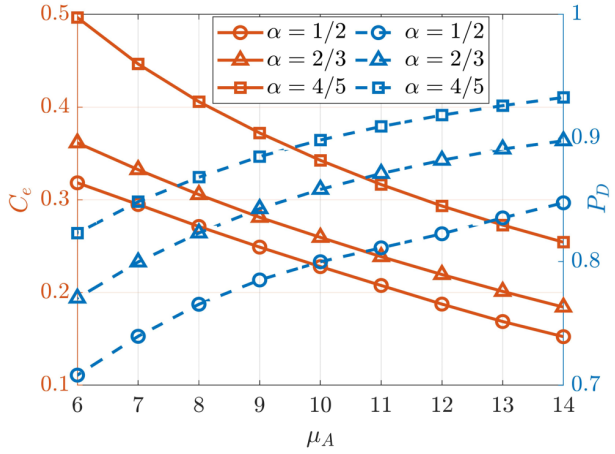

Figure 6. C_e and $P_D(\epsilon_0)$ under different μ_A and α.

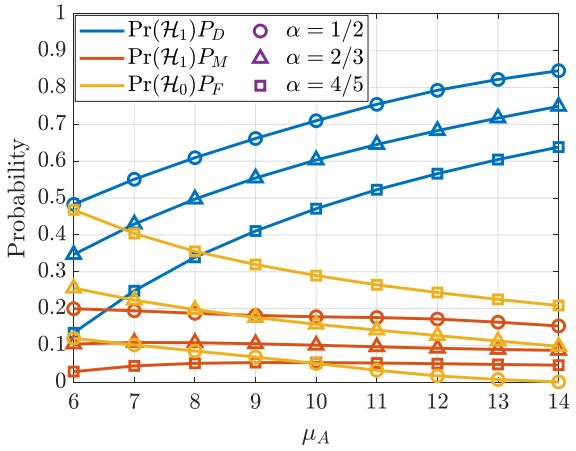

Figure 7. $\Pr(\mathcal{H}_1)P_D(\epsilon_0)$, $\Pr(\mathcal{H}_1)P_M(\epsilon_0)$, and $\Pr(\mathcal{H}_0)P_F(\epsilon_0)$ under different μ_A and α.

6. Conclusions

In this paper, the theoretical foundations of connectivity-based mobility detection were developed by defining and deriving $P_D(\epsilon)$, $P_M(\epsilon)$, and $P_F(\epsilon)$ in terms of a mobility detection threshold ϵ under the shadow fading channel and arbitrary mobility models. The determination of the optimal detection threshold was made with respect to the anchor number from the perspective of the average error cost minimization. Through the

numerical evaluations, we showed that the detection resolution and the mobility detection probability are improved by increasing the number of anchors, and that the probabilities are bounded by the costs of miss detection and false alarm, which was also theoretically proven. We believe that our results can be used as potential foundations upon which others facilitate the design, development, and deployment of connectivity-based localization supporting mobility.

Author Contributions: Conceptualization, S.L. and S.K. (Sunwoo Kim); methodology, S.L. and S.K. (Sungjin Kim); software, I.B. and S.K. (Sungjin Kim); validation, S.L., I.B., S.K. (Sungjin Kim) and S.K. (Sunwoo Kim); formal analysis, I.B. and S.K. (Sungjin Kim); investigation, I.B. and S.K. (Sungjin Kim); resources, I.B. and S.K. (Sungjin Kim); data curation, S.L.; writing—original draft preparation, S.L. and S.K. (Sungjin Kim); writing—review and editing, S.L., I.B. and S.K. (Sunwoo Kim); visualization, S.K. (Sungjin Kim); supervision, S.L. and S.K. (Sunwoo Kim); project administration, S.K. (Sunwoo Kim); funding acquisition, S.K. (Sunwoo Kim). All authors have read and agreed to the published version of the manuscript.

Funding: This work was supported in part by the ICT Research and Development Program of MSIP/IITP (Standard technology development and its international standardization for T2X services based on 5G) under Grant 2020-0-00505.

Conflicts of Interest: The authors declare no conflict of interest.

Abbreviations

The following abbreviations are used in this manuscript:

BLE	Bluetooth Low Energy
CDF	Cumulative Distribution Function
DV-Hop	Distance Vector-Hop
IoT	Internet-of-Things
ITU	International Telecommunication Union
MCL	Monte Carlo Localization
PDF	Probability Density Function
UDG	Unit Disk Graph

Appendix A. Proof of (15)

Assuming $F_Z(\epsilon) \approx 1$, $f_Z(z_n)$ is approximated to zero when $z_n \geq \epsilon$. From the L'Hospital's rule, $P_D(\epsilon)$ in (8) and $P_M(\epsilon)$ in (9) can be expressed as follows:

$$\begin{aligned}\lim_{F_Z(\epsilon)\to 1} P_D(\epsilon) &= 1 - \lim_{F_Z(\epsilon)\to 1} \frac{\int_\epsilon^\infty f_Z(z_n)\exp\{\mu_A(h(z_n)-1)\}\,dz_n}{1-F_Z(\epsilon)} \\ &= 1 - \lim_{F_Z(\epsilon)\to 1} \frac{f_Z(\epsilon)\exp\{\mu_A(h(\epsilon)-1)\}}{f_Z(\epsilon)} \\ &= 1 - \exp\{\mu_A(h(\epsilon)-1)\}.\end{aligned} \tag{A1}$$

$$\lim_{F_Z(\epsilon)\to 1} P_M(\epsilon) = \lim_{F_Z(\epsilon)\to 1} (1 - P_D(\epsilon)) = \exp\{\mu_A(h(\epsilon)-1)\}. \tag{A2}$$

Appendix B. Proof of (18)

Assuming $F_Z(\epsilon) \approx 0$, $f_Z(z_n)$ is approximated to zero when $0 \leq z_n \leq \epsilon$. From the L'Hospital's rule, $P_F(\epsilon)$ in (10) can be expressed as follows:

$$\begin{aligned}\lim_{F_Z(\epsilon)\to 0} P_F(\epsilon) &= 1 - \lim_{F_Z(\epsilon)\to 0} \frac{\int_0^\epsilon f_Z(z_n)\exp\{\mu_A(h(z_n)-1)\}\,dz_n}{F_Z(\epsilon)} \\ &= 1 - \lim_{F_Z(\epsilon)\to 0} \frac{f_Z(\epsilon)\exp\{\mu_A(h(\epsilon)-1)\}}{f_Z(\epsilon)} \\ &= 1 - \exp\{\mu_A(h(\epsilon)-1)\}.\end{aligned} \tag{A3}$$

References

1. Wang, X.; Wang, Z.; O'Dea, B. A TOA-based location algorithm reducing the errors due to non-line-of-sight (NLOS) propagation. *IEEE Trans. Veh. Technol.* **2003**, *52*, 112–116. [CrossRef]
2. Laoudias, C.; Moreira, A.; Kim, S.; Lee, S.; Wirola, L.; Fischione, C. A survey of enabling technologies for network localization, tracking, and navigation. *IEEE Commun. Surv. Tutor.* **2018**, *20*, 3607–3644. [CrossRef]
3. Wang, Z.; Zhang, H.; Lu, T.; Gulliver, T.A. A grid-based localization algorithm for wireless sensor networks using connectivity and RSS rank. *IEEE Access* **2018**, *6*, 8426–8439. [CrossRef]
4. Burda, R.; Lewandowski, A.; Wietfeld, C. A hybrid indoor localization using beacon enabled meshing and TOA in IEEE 802.15.4 networks. In Proceedings of the IEEE Vehicular Technology Conference (VTC) Spring, Marina Bay, Singapore, 11–14 May 2008; pp. 118–122.
5. Bulusu, N.; Heidemann, J.; Estrin, D. GPS-less low-cost outdoor localization for very small devices. *IEEE Pers. Commun.* **2000**, *7*, 28–34. [CrossRef]
6. Niculescu, D.; Nath, B. Ad hoc positioning system (APS). In Proceedings of the IEEE Global Telecommunications Conference (GLOBECOM), San Antonio, TX, USA, 25–29 November 2001; Volume 5, pp. 2926–2931.
7. Lee, S.; Jin, M.; Koo, B.; Sin, C.; Kim, S. Pascal's triangle-based range-free localization for anisotropic wireless networks. *Wirel. Netw.* **2016**, *22*, 2221–2238. [CrossRef]
8. Wang, Y.; Wang, X.; Wang, D.; Agrawal, D.P. Range-free localization using expected hop progress in wireless sensor networks. *IEEE Trans. Parallel Distrib. Syst.* **2009**, *20*, 1540–1552. [CrossRef]
9. Xiao, Q.; Xiao, B.; Cao, J.; Wang, J. Multihop range-free localization in anisotropic wireless sensor networks: A pattern-driven scheme. *IEEE Trans. Mob. Comput.* **2010**, *9*, 1592–1607. [CrossRef]
10. Xiao, B.; Chen, L.; Xiao, Q.; Li, M. Reliable anchor-based sensor localization in irregular areas. *IEEE Trans. Mob. Comput.* **2009**, *9*, 60–72. [CrossRef]
11. Lee, S.; Lee, D.; Lee, C. Enhanced DV-Hop algorithm with reduced hop-size error in ad hoc networks. *IEICE Trans. Commun.* **2011**, *E94.B*, 2130–2132. [CrossRef]
12. Zhao, J.; Xi, W.; He, Y.; Liu, Y.; Li, X.; Mo, L.; Yang, Z. Localization of wireless sensor networks in the wild: Pursuit of ranging quality. *IEEE/ACM Trans. Netw.* **2013**, *21*, 311–323. [CrossRef]
13. Assaf, A.E.; Zaidi, S.; Affes, S.; Kandil, N. Range-free localization algorithm for heterogeneous Wireless Sensor Networks. In Proceedings of the IEEE Wireless Communications and Networking Conference (WCNC), Istanbul, Turkey, 6–9 April 2014; pp. 2805–2810.
14. Chen, J.; Zhang, W.; Liu, Z.; Wang, R.; Zhang, S. CWDV-Hop: A hybrid localization algorithm with distance-weight DV-Hop and CSO for wireless sensor networks. *IEEE Access* **2021**, *9*, 380–399. [CrossRef]
15. Li, M.; Liu, Y. Rendered Path: Range-free localization in anisotropic sensor networks with holes. *IEEE/ACM Trans. Netw.* **2010**, *18*, 320–332.
16. Lee, S.; Park, C.; Lee, M.J.; Kim, S. Multihop range-free localization with approximate shortest path in anisotropic wireless sensor networks. *EURASIP J. Wirel. Commun. Netw.* **2014**, *2014*, 80. [CrossRef]
17. Sheu, J.; Chen, P.; Hsu, C. A distributed localization scheme for wireless sensor networks with improved grid-scan and vector-based refinement. *IEEE Trans. Mob. Comput.* **2008**, *7*, 1110–1123. [CrossRef]
18. Lee, S.; Woo, H.; Lee, C. Wireless sensor network localization with connectivity-based refinement using mass spring and Kalman filtering. *EURASIP J. Wirel. Commun. Netw.* **2012**, *2012*, 152. [CrossRef]
19. Gui, L.; Xiao, F.; Zhou, Y.; Shu, F.; Val, T. Connectivity based DV-Hop localization for Internet of Things. *IEEE Trans. Veh. Technol.* **2020**, *69*, 8949–8958. [CrossRef]
20. Liu, X.; Zhang, S.; Wang, J.; Cao, J.; Xiao, B. Anchor supervised distance estimation in anisotropic wireless sensor networks. In Proceedings of the IEEE Wireless Communications and Networking Conference (WCNC), Cancun, Mexico, 28–31 March 2011; pp. 938–943.
21. Woo, H.; Lee, C.; Oh, S. Reliable anchor node based range-free localization algorithm in anisotropic wireless sensor networks. In Proceedings of the International Conference on Information Networking (ICOIN), Bangkok, Thailand, 27–30 January 2013; pp. 618–622.
22. Lee, S.; Koo, B.; Kim, S. RAPS: Reliable anchor pair selection for range-free localization in anisotropic networks. *IEEE Commun. Lett.* **2014**, *18*, 1403–1406. [CrossRef]
23. Saeed, N.; Nam, H.; Al-Naffouri, T.Y.; Alouini, M. A state-of-the-art survey on multidimensional scaling-based localization techniques. *IEEE Commun. Surv. Tutor.* **2019**, *21*, 3565–3583. [CrossRef]
24. Zazali, A.A.; Subramaniam, S.K.; Zukarnain, Z.A. Flood control distance vector-hop (FCDV-Hop) localization in wireless sensor networks. *IEEE Access* **2020**, *8*, 206592–206613. [CrossRef]
25. Hu, L.; Evans, D. Localization for mobile sensor networks. In Proceedings of the 10th Annual International Conference Mobile Computing Networking (MobiCom), Philadelphia, PA, USA, 26 September-1 October 2004; pp. 45–57.
26. Gao, D.; Chen, P.; Foh, C.H.; Niu, Y. Hop-distance relationship analysis with quasi-UDG model for node localization in wireless sensor networks. *EURASIP J. Wirel. Commun. Netw.* **2011**, *2011*, 99. [CrossRef]
27. Baggio, A.; Langendoen, K. Monte Carlo localization for mobile wireless sensor networks. *Ad-hoc Netw.* **2008**, *6*, 718–733. [CrossRef]

28. Rudafshani, M.; Datta, S. Localization in wireless sensor networks. In Proceedings of the 6th IEEE International Symposium Information Processing Sensor Networks (IPSN), Cambridge, MA, USA, 25–27 April 2007; pp. 51–60.
29. Sheu, J.P.; Hu, W.K.; Lin, J.C. Distributed localization scheme for mobile sensor networks. *IEEE Trans. Mob. Comput.* **2010**, *9*, 516–526. [CrossRef]
30. Zhang, S.; Cao, J.; Li-Jun, C.; Chen, D. Accurate and energy-efficient range-free localization for mobile sensor networks. *IEEE Trans. Mob. Comput.* **2010**, *9*, 897–910. [CrossRef]
31. Bochem, A.; Yuan, Y.; Hogrefe, D. Tri-MCL: Synergistic localization for mobile ad-hoc and wireless sensor networks. In Proceedings of the IEEE 41st Conf. Local Computer Networks (LCN), Dubai, United Arab Emirates, 7–10 November 2016; pp. 333–338.
32. Wang, Z.; Wang, Y.; Ma, M.; Wu, J. Efficient localization for mobile sensor networks based on constraint rules optimized Monte Carlo method. *Comput. Netw.* **2013**, *57*, 2788–2801. [CrossRef]
33. Huang, J.F.; Chang, G.Y.; Chen, G.H. A historical-beacon-aided localization algorithm for mobile sensor networks. *IEEE Trans. Mob. Comput.* **2014**, *14*, 1109–1122. [CrossRef]
34. Nagpal, R.; Shrobe, H.; Bachrach, J. Organizing a global coordinate system from local information on an ad hoc sensor network. In Proceedings of the 2nd International Workshop on Information Processing in Sensor Networks (IPSN), Palo Alto, CA, USA, 22–23 April 2003; pp. 333–348.
35. MacLean, S.; Datta, S. A lower bound on range-free node localization algorithms. In Proceedings of the IEEE International Symposium on Wireless Commun. Systems (ISWCS), Reykjavik, Iceland, 21–24 October 2008; pp. 628–632.
36. Chan, Y.W.E.; Soong, B.H. A new lower bound on range-free localization algorithms in wireless sensor networks. *IEEE Commun. Lett.* **2010**, *15*, 16–18. [CrossRef]
37. Gui, L.; He, B.; Xiao, F.; Shu, F. Resolution limit of positioning error for range-free localization schemes. *IEEE Syst. J.* **2020**, *14*, 2980–2989. [CrossRef]
38. Goldsmith, A. *Wireless Communications*; Cambridge University Press: Cambridge, UK, 2005.
39. Nikoukar, A.; Abboud, M.; Samadi, B.; Güneş, M.; Dezfouli, B. Empirical analysis and modeling of Bluetooth low-energy (BLE) advertisement channels. In Proceedings of the 17th Annual Mediterranean Ad Hoc Networking Workshop (Med-Hoc-Net), Capri, Italy, 20–22 June 2018; pp. 1–6.
40. Spachos, P.; Plataniotis, K.N. BLE beacons for indoor positioning at an interactive IoT-based smart museum. *IEEE Syst. J.* **2020**, *14*, 3483–3493. [CrossRef]
41. *Propagation Data and Prediction Methods for the Planning of Indoor Radiocommunication Systems and Radio Local Area Networks in the Frequency Range 300 MHz to 450 GHz*; Recommendation ITU-R P.1238-10; International Telecommunication Union: Geneva, Switzerland, 2019.
42. *Propagation Data and Prediction Methods for the Planning of Short-Range Outdoor Radiocommunication Systems and Radio Local area Networks in the Frequency Range 300 MHz to 100 GHz*; Recommendation ITU-R P.1411-10; International Telecommunication Union: Geneva, Switzerland, 2019.
43. Bluetooth SIG, Inc. 3 Key Factors That Determine the Range of Bluetooth. Available online: https://www.bluetooth.com/blog/3-key-factors-that-determinethe-range-of-bluetooth/ (accessed on 15 January 2021).
44. Sum, C.S.; Zhou, M.T.; Kojima, F.; Harada, H. Experimental performance evaluation of multihop IEEE 802.15.4/4g/4e smart utility networks in outdoor environment. *Wirel. Commun. Mob. Comput.* **2017**, *2017*, 7137406. [CrossRef]
45. Behnad, A.; Wang, X.; Hanzo, L.; Willink, T.J. Connectivity-based centroid localization using distributed dense reference nodes. *IEEE Trans. Veh. Technol.* **2018**, *67*, 6685–6689. [CrossRef]
46. Fascista, A.; Ciccarese, G.; Coluccia, A.; Ricci, G. A change-detection approach to mobile node localization in bounded domains. In Proceedings of the 52nd Annual Conference on Information Sciences and Systems (CISS), Princeton, NJ, USA, 21–23 March 2018; pp. 1–6.
47. Robinson, M.; Ghrist, R. Topological localization via signals of opportunity. *IEEE Trans. Signal Process.* **2012**, *60*, 2362–2373. [CrossRef]
48. Camp, T.; Boleng, J.; Davies, V. A survey of mobility models for ad hoc network research. *Wirel. Commun. Mob. Comput.* **2002**, *2*, 483–502. [CrossRef]
49. Vuran, M.C.; Akan, Ö.B.; Akyildiz, I.F. Spatio-temporal correlation: Theory and applications for wireless sensor networks. *Comput. Netw.* **2004**, *45*, 245–259. [CrossRef]